

# Assessment of Triboelectricity in Colossal-Surface-Area-Lanthanum Oxide Nanocrystals Synthesized via Low-Temperature Hydrothermal Process

SUNIL METI

NITK Surathkal: National Institute of Technology Karnataka

Hosangadi Prutvi Sagar

IIT Bombay: Indian Institute of Technology Bombay

Mohammad Rizwanur Rahman

NITK Surathkal: National Institute of Technology Karnataka

Udaya Bhat K (✉ [udayabhatk@gmail.com](mailto:udayabhatk@gmail.com))

National Institute of Technology Karnataka <https://orcid.org/0000-0002-0752-3600>

---

## Research Article

**Keywords:** Hydrothermal method, X-ray methods, Spectroscopy, Triboelectric properties

**Posted Date:** February 24th, 2021

**DOI:** <https://doi.org/10.21203/rs.3.rs-233671/v1>

**License:**  This work is licensed under a Creative Commons Attribution 4.0 International License.

[Read Full License](#)

---

**Version of Record:** A version of this preprint was published at Journal of Materials Science: Materials in Electronics on July 14th, 2021. See the published version at <https://doi.org/10.1007/s10854-021-06545-7>.

# Abstract

Triboelectric nanogenerators (TENGs) have marked their applications in various fields, most importantly, in medical devices. The electrical output of the TENGs mainly concentrated on parameters such as electrode separation distance, applied mechanical pressure, surface charge density, and overlapping surface-area. The surface-area of the active layer in TENGs plays a crucial role. Given this, the present contribution is the first report on the utilization of lanthanum oxide ( $\text{La}_2\text{O}_3$ ) as an active material with a large surface-area ( $\sim 72.33 \text{ m}^2/\text{g}$ ) in TENGs. The nanocrystals of  $\text{La}_2\text{O}_3$  have been successfully embedded into TENGs architecture through a high-quality screen-printed film with a Teflon-counter surface. The in-house test-rig of TENGs resulted in an output open-circuit voltage of 120 V and a short-circuit current of 23.7  $\mu\text{A}$ . Further, the maximum power density is 7.125  $\text{W}/\text{m}^2$  at an external load resistance of 30  $\text{M}\Omega$ . These results suggest that  $\text{La}_2\text{O}_3$  is a suitable contender in various self-powered devices.

## 1. Introduction

The increased human dependency on portable electronic gadgets resulted in the high demand for the energy sources, such as batteries and other storage devices. Thus, the demand for low powered and self-powered devices making their mark worldwide. The replacement of conventional devices along with powering sources by self-powered may address the energy crises for a large extent. In view of this, the triboelectric nanogenerators (TENGs) play a crucial role which harvests naturally occurring energy as a power source. The advantages of TENGs are not only the low cost production but also simple and economic fabrication of the devices. The triboelectric device works on the principle of conjunction of tribo-electrification and electrostatic induction [1]. The recent reports on active materials for TENGs have mainly focused to enhance the performance by morphology tuning, fabrication methods and selecting the best materials [2–7]. The recent reports focused mainly on tribo-active materials like zinc oxide (ZnO), polyvinylidene fluoride (PVDF), polyimide aerogel, *etc.* [8][9]. There were less or no reports on TENGs using  $\text{La}_2\text{O}_3$  as active material. Hence, the study is focused mainly on TENGs based on  $\text{La}_2\text{O}_3$ .

Lanthanum has been widely explored in its compound states such as oxides, hydroxides as well as phosphate forms. Numerous techniques for synthesizing the lanthanum oxide nanoparticles have been proposed, such as thermal decomposition, homogeneous precipitation, solvothermal, hydrothermal and other chemical routes [10]. From the literature, it is shown that there are many reports on microwave-assisted hydrothermal synthesis and surfactant-assisted  $\text{La}_2\text{O}_3$  nanorods, nanoneedles and nanorod bundles [11][10]. Solution phase synthesis favors the agglomeration and spherical particle formation because of its high surface energy. To reduce the agglomeration of the 1D lanthanum oxide nanoparticles, suitable capping agents like surfactants, polymers, or templates were employed [12].

Lanthanum oxide is a ceramic material and is brittle in nature. Lanthanum and its compounds have been widely used in optical, electrical, magnetic materials and the most importantly in impurity extraction, such

as arsenic (As (III)) [13][14]. Recent literature on the  $\text{La}_2\text{O}_3$  materials have revealed that it could be used in solid fuel cells, high-temperature superconductors [15][16]. Lanthanum oxide has found great attention in the area of piezoelectric materials, thermoelectric materials, automobile exhaust-gas convectors, optoelectronic devices, sensors, catalysis, and solid electrolyte [14][17].

The exploration of such lanthanum oxide architectures have opened an area of interest for innovative ceramic-metal oxide nanoparticles with tuneable materials properties like electronic, magnetic and catalytic properties [18–20]. The piezoelectric nature of the  $\text{La}_2\text{O}_3$  material favors its application in the area of self-powered devices.

In this work, a single-step hydrothermal synthesis of  $\text{La}_2\text{O}_3$  nanocrystals is presented. The processing is of simple, cost effective and demands a minimal thermal budget. The  $\text{La}_2\text{O}_3$  nanocrystals synthesized with this technique processes uniform morphology and size distribution. The synthesized  $\text{La}_2\text{O}_3$  nanocrystals are characterized to study its morphological and structural properties. The synthesized nanocrystals are grounded with suitable capping agent to form paste for the screen printing technique without modifying its base properties. The  $\text{La}_2\text{O}_3$  film is fabricated using synthesized nanocrystals and suitable reagents by the screen printing technique. The prepared film is then examined to study the triboelectric properties.

## 2. Materials And Methods

### 2.1. Hydrothermal synthesis of $\text{La}_2\text{O}_3$ nanocrystals

A known weight of (1.4 g) cetyl trimethyl ammonium bromide (CTAB) is added to 100 ml of de-ionized (DI) water. The solution is stirred vigorously for a few minutes. Then, 3 g of lanthanum chloride ( $\text{LaCl}_3$ ) salt is added to the solution and stirred continuously using magnetic bar. 3 ml of 25% ammonia ( $\text{NH}_3$ ) solution is added drop-wise to the solution to maintain a basic pH ranging between 9 - 10. The resultant solution is stirred for 12 h and made in to colloidal dispersion with a translucent appearance. The prepared solution is poured into 200 ml stainless steel autoclave and kept in an oven at 100 °C for 48 h. The products obtained post heat treatment is then rinsed with DI water and ethanol several times to annihilate the residuals. Finally, the  $\text{La}_2\text{O}_3$  nanocrystals are subjected for drying in an oven at 80 °C for 24 h. The dried product- $\text{La}_2\text{O}_3$  is stored in an air-tight bottle to avoid moisture contamination.

### 2.2. Screen printing of $\text{La}_2\text{O}_3$ film

45 weight percent (45 wt.%) of as-synthesized  $\text{La}_2\text{O}_3$  nanocrystals are mixed with 5 wt.% of ethylcellulose binder and 50 wt.% of terpinol solvent. The mixture is then grounded rigorously in Mortar-pestle for 30 min to get high viscous agglomeration-free  $\text{La}_2\text{O}_3$  screen printable paste. The mask for screen printing is created using a screen with #120 mesh. The snap-off distance of 5-10 mm is maintained to facilitate the quick release of the screen. The copper adhesive tape cleaned with isopropyl alcohol, acetone, and DI water, is used as a substrate for screen printing. Here, the copper adhesive tape is flexible, which helps in

device fabrication and testing, and also acts as an electrode. The films are then dried under infrared (IR) radiation for three to four hours to ensure the complete evaporation of the solvent.

### 2.3. Characterization

The X-ray diffractometry (XRD, make-JEOL-JPZ-8 with a copper target ( $\text{Cu K}\alpha = 1.54 \text{ \AA}$ )) is used for the examination of phase purification of the  $\text{La}_2\text{O}_3$  nanocrystals. The chemical nature of  $\text{La}_2\text{O}_3$  nanocrystals is studied by using X-ray photoelectron spectroscopy (XPS- Kratos Analytical, UK, monochromatic  $\text{Al K}\alpha \sim 1486.6 \text{ eV}$  as X-ray source and XPS; PHI5000VersaProbell). Prior to the XPS measurements, the sample is treated under argon gas to eliminate the surface impurities. The calibration of all the XPS data are performed with the standard reference carbon  $1s$  ( $\text{C } 1s$ ) peak at  $284.7 \text{ eV}$  and  $\pm 0.2 \text{ eV}$  of accuracy is maintained for measuring the binding energies. The deconvolution of oxygen  $1s$  ( $\text{O } 1s$ ) and lanthanum  $3d$  ( $\text{La } 3d$ ) is performed after the subtraction of the background using Shirley function. Further, the addition of synthetic peaks is performed using Gaussian-Lorentzian peak function with area resolution of  $1 \text{ eV}$ . The nature and surface morphologies of the  $\text{La}_2\text{O}_3$  nanocrystals are examined by using field emission scanning electron microscopy (FESEM, make-JEOL-JSM-6380LA, Tokyo, Japan) and transmission electron microscopy (TEM, JEOL-JEM-2100, Tokyo Japan). A very minute amount of  $\text{La}_2\text{O}_3$  nanocrystals dispersed in ethanol and a drop of prepared colloidal solution is poured on carbon-coated copper grid. Finally, the grid is dried under bulb (60 W). The grid containing  $\text{La}_2\text{O}_3$  nanocrystals is then subjected for TEM examination. The Fourier transform infrared (FTIR, make-JASCO-4200 spectrometer, in KBr mode) is used to study the quality and the formation of  $\text{La}_2\text{O}_3$  nanocrystals. The Brunauer-Emmett-Teller (BET) apparatus is used for the calculation of specific surface-area of  $\text{La}_2\text{O}_3$  nanocrystals following the standard protocols at  $77 \text{ K}$ . Prior to the BET measurements, the  $\text{La}_2\text{O}_3$  nanocrystals are degassed in presence of flowing  $\text{N}_2$  at  $300 \text{ }^\circ\text{C}$  for  $12 \text{ h}$  [21].

To evaluate the triboelectric performance, the screen-printed film is tested in a in-house built motorized fixture as shown in the Fig. 1. The dimension of the screen-printed  $\text{La}_2\text{O}_3$  TENG device is ( $2.5 \text{ cm} \times 2.5 \text{ cm}$ ). Teflon is used as a counter surface for testing the  $\text{La}_2\text{O}_3$  TENG device, since it is fluorine rich, leading to high electronegativity. The thickness of the Teflon used is  $0.25 \text{ mm}$ . Before the measurement of triboelectric response, the  $\text{La}_2\text{O}_3$  screen-printed film thickness is measured to be  $10 \text{ }\mu\text{m}$  with average surface roughness of  $0.25 \text{ }\mu\text{m}$ . While testing, the fixture is operated at around  $15 \text{ Hz}$  with applied maximum load of approximately  $300 \text{ g}$  at the hetero junction. The electrical parameters (i.e., voltage and current) are logged using an oscilloscope (Tektronix DPO 2014B) and Keithley parameter analyzer (4200s), respectively.

## 3. Results And Discussion

### 3.1. Surface morphology of $\text{La}_2\text{O}_3$ nanocrystals

The micrographs of  $\text{La}_2\text{O}_3$ , captured from a scanning electron microscope (Fig. 2. (a-b)) depicts the rod-like morphology. The synthesized  $\text{La}_2\text{O}_3$  nanocrystals are uniform in size and shape, showing its homogeneous formation during the synthesis. The micrographs at different locations present the uniform morphology with dimensions varying in few hundreds of nanometers.

The diameter of the  $\text{La}_2\text{O}_3$  nanocrystals is in the range of 5 to 30 nm and length is 100 to 300 nm (Fig. 2. (a & b)). Fig. 2c shows the TEM micrograph of the  $\text{La}_2\text{O}_3$  nanocrystals, corresponding high-resolution image (Fig. 2d) and SAED ring pattern (Fig. 2e). The TEM analysis shows the crystalline structure of  $\text{La}_2\text{O}_3$ . The interplanar spacing is 0.334 nm (from Fig. 2d). The ring pattern with intense spot in Fig. 2e, the  $\text{La}_2\text{O}_3$  nanocrystals showed the intense diffraction spots suggesting the particles formed.

### 3.2. Crystal structure of $\text{La}_2\text{O}_3$ using XRD

The XRD of hydrothermally synthesized  $\text{La}_2\text{O}_3$  nanocrystals is shown in Fig. 3. The synthesized  $\text{La}_2\text{O}_3$  nanocrystals are of high purity and pattern indexed with hexagonal phase (space group  $P-3m1$ , ICDD No. 83-1344) [22].

The sharp diffraction peaks at respective Bragg angles indicate that the high crystallinity achieved at considerably low-temperatures. Thus, both morphological and structural analysis concludes the quality of the synthesized nanocrystals. Also, the broad peaks with large FWHM depict the nanocrystalline nature, which is in good agreement with high-resolution TEM studies presented in Fig. 2 (c-d).

### 3.3. Chemical composition of $\text{La}_2\text{O}_3$ nanocrystals using XPS

Further, the  $\text{La}_2\text{O}_3$  sample is subjected for XPS study to examine the composition. All the binding energy data of  $\text{La}_2\text{O}_3$  sample obtained from the XPS analysis is corrected according to the standard referencing C 1s peak (284.7 eV). From Fig. 4a, the XPS survey spectrum shows only the presence of two metal elements, lanthanum and oxygen. The survey also shows that there is no presence of other metal elements on the surface of  $\text{La}_2\text{O}_3$  sample. The presence of minor C 1s peak (Fig. 4a) is due to the surface adsorbed carbon atoms/molecules during the hydrothermal synthesis. The binding energy at 833.6 and 850.1 eV are indexed to the presence of La  $3d_{5/2}$  and La  $3d_{3/2}$ , respectively, as shown in Fig. 4b. The binding energy peak at 529.5 eV, in Fig. 4c, is indexed to the  $\text{O}^{2-}$  in the  $\text{La}_2\text{O}_3$  crystal. It is also seen that the O 1s profile is asymmetric indicating the presence of two oxygen species in the nearby region.

### 3.4. BET surface area analysis

Brunauer–Emmett–Teller (BET) nitrogen gas adsorption-desorption measurements are used to find out the specific surface area of the  $\text{La}_2\text{O}_3$  nanocrystals. The isotherm shows that the particles are porous (Fig. 5). The specific surface area of  $\text{La}_2\text{O}_3$  from the BET apparatus is measured to be 72.33  $\text{m}^2/\text{g}$ . The value is predominant compared to already published literatures [23] [24] [25].

### 3.5. Identification of chemical bonding by FTIR

The FTIR spectrum is recorded to show the functional groups of the  $\text{La}_2\text{O}_3$  nanocrystals (as shown in Fig. 6). The stretching vibration of O-H bond at  $3427\text{ cm}^{-1}$  and the bending vibration of H-O-H absorption peak at  $1631\text{ cm}^{-1}$  are due to the presence of moisture in  $\text{La}_2\text{O}_3$  sample [26]. The absorption band at  $3608\text{ cm}^{-1}$  is assigned to the presence of bond tension in hydroxyl groups of lanthanum oxide. Further, the bands at  $1483\text{ cm}^{-1}$  and  $1440\text{ cm}^{-1}$  are attributed to asymmetric stretching mode of the C-O bond [22]. The absorption bands at  $858$  and  $657\text{ cm}^{-1}$  are assigned to bending out of plane vibrations and La-O stretching vibration, respectively [27].

### 3.6. Output characteristics of triboelectric nanogenerators

To evaluate the maximum power generated by the device, TENG device is connected to an electrical load (resistor)s [28]. The obtained voltage is as shown in the Fig. 7. The resistance value is swept from 0 to 50 M $\Omega$ . Respective voltage and current produced by the  $\text{La}_2\text{O}_3$ -TENG device are plotted against the external load resistance. The product of the same (i.e., voltage and current) gives the power value as is found to be maximum at the point where current and voltage intersect each other at 30 M $\Omega$ .

The current amplitude reduces with growing external load resistance owing to resistive loss, during which the voltage increases. Oscilloscope is used to record the voltage and current generated by  $\text{La}_2\text{O}_3$ -TENG device. The performance of the device is tested by tapping the TENG using the motorized fixture (Fig. 1). The phenomenon of chemisorptions on the surface of teflon and  $\text{La}_2\text{O}_3$  film surface of molecular oxygen species results in resistivity changes of triboelectric material [29,30]. When Teflon and  $\text{La}_2\text{O}_3$  nanorods film come into contact, spontaneous polarization occurs [31]. This result in the dipole moments on teflon film and  $\text{La}_2\text{O}_3$  surface and thus voltage generates. The open-circuit voltage and short circuit produced by the  $\text{La}_2\text{O}_3$ -TENG device is 120 V and 23.7  $\mu\text{A}$ . The device yields a maximum power of 2.85 mW at an external load resistance of 30 M $\Omega$  (Fig. 7). The corresponding power density of the  $\text{La}_2\text{O}_3$  TENG device is calculated to be 7.125 W/m<sup>2</sup>.

## Conclusions

The synthesis of high surface area ( $\sim 72.33\text{ m}^2/\text{g}$ )  $\text{La}_2\text{O}_3$  nanocrystals using the hydrothermal technique is presented with its direct utilization in the form of screen-printed film in TENGs. Further, TEM-SAED pattern of  $\text{La}_2\text{O}_3$  nanocrystals showed high intense diffraction spots conclude that the particles were crystallized. FTIR analysis showed the presence of La-O bond. XPS analysis showed the chemical nature of the nanocrystals. The film of  $\text{La}_2\text{O}_3$  was investigated for its triboelectric behavior and the results depict that the peak output power density could reach up to 7.125 W/m<sup>2</sup> at load resistor of 30 M $\Omega$ . Thus these results depicts that  $\text{La}_2\text{O}_3$  film TENG device could be used for the self-powered devices and many improvements could be done to improve the power density to use it in various energy harvesting applications.

# Declarations

## Acknowledgement

The authors are thankful to Ms. Rashmi for her help taking in SEM micrographs. The authors would also like to thank the “Central Surface Analytical Facility of IIT Bombay” for the assistance in XPS characterization.

## Conflict of interest

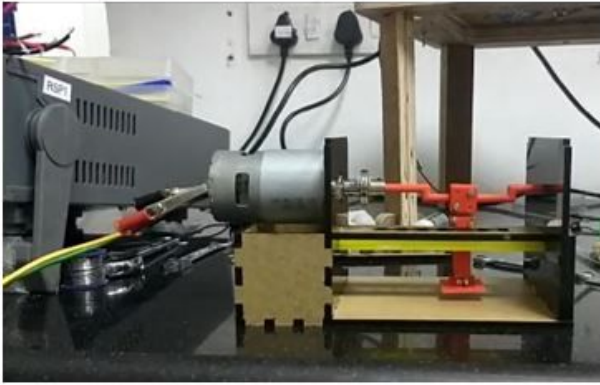
The authors have no conflict of interest.

## References

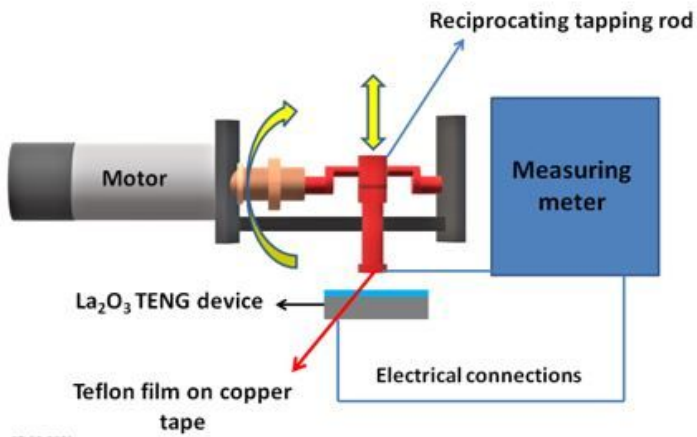
1. Q. Liang, Q. Zhang, X. Yan, X. Liao, L. Han, F. Yi, M. Ma, and Y. Zhang, *Adv. Mater.* **29**, (2017).
2. H. Y. Mi, X. Jing, Q. Zheng, L. Fang, H. X. Huang, L. S. Turng, and S. Gong, *Nano Energy* **48**, 327 (2018).
3. Z. Saadatnia, S. G. Mosanenzadeh, T. Li, E. Esmailzadeh, and H. E. Naguib, *Nano Energy* **65**, (2019).
4. H. Y. Mi, X. Jing, M. A. B. Meador, H. Guo, L. S. Turng, and S. Gong, *ACS Appl. Mater. Interfaces* **10**, 30596 (2018).
5. Y. Tang, Q. Zheng, B. Chen, Z. Ma, and S. Gong, *Nano Energy* **38**, 401 (2017).
6. H. Wang, M. Shi, K. Zhu, Z. Su, X. Cheng, Y. Song, X. Chen, Z. Liao, M. Zhang, and H. Zhang, *Nanoscale* **8**, 18489 (2016).
7. S. H. Ramaswamy, J. Shimizu, W. Chen, R. Kondo, and J. Choi, *Nano Energy* **60**, 875 (2019).
8. B. Zhang, L. Zhang, W. Deng, L. Jin, F. Chun, H. Pan, B. Gu, H. Zhang, Z. Lv, W. Yang, and Z. L. Wang, *ACS Nano* **11**, 7440 (2017).
9. Z. Saadatnia, S. G. Mosanenzadeh, E. Esmailzadeh, and H. E. Naguib, *Sci. Rep.* **9**, (2019).
10. J. Sheng, S. Zhang, S. Lv, and W. Sun, in *J. Mater. Sci.* (2007), pp. 9565–9571.
11. A. V. Murugan and A. K. Viswanath, *J. Phys. D. Appl. Phys.* **39**, 3974 (2006).
12. C. J. Murphy, T. K. Sau, A. M. Gole, C. J. Orendorff, J. Gao, L. Gou, S. E. Hunyadi, and T. Li, *J. Phys. Chem. B* **109**, 13857 (2005).
13. J. W. Stouwdam, G. A. Hebbink, J. Huskens, and F. C. J. M. Van Veggel, *Chem. Mater.* **15**, 4604 (2003).
14. Y. Xiao, Z. Feng, X. Huang, L. Huang, Z. Long, Q. Wang, and Y. Hou, *Chinese Sci. Bull.* **59**, 1864 (2014).
15. P. Allenspach and U. Gasser, *J. Alloys Compd.* **311**, 1 (2000).
16. J. Zhang, Z. Zhang, Y. Jiao, H. Yang, Y. Li, J. Zhang, and P. Gao, *J. Power Sources* **419**, 99 (2019).
17. L. Kong, Y. Tian, N. Li, Y. Liu, J. Zhang, J. Zhang, and W. Zuo, *Appl. Clay Sci.* **162**, 507 (2018).
18. M. Ghiasi and A. Malekzadeh, *Superlattices Microstruct.* **77**, 295 (2015).

19. Q. Mu and Y. Wang, *J. Alloys Compd.* **509**, 396 (2011).
20. M. Salavati-Niasari, G. Hosseinzadeh, and F. Davar, *J. Alloys Compd.* **509**, 4098 (2011).
21. S. Sivasankaran and M. J. Kishor Kumar, *Ceram. Int.* **41**, 11301 (2015).
22. M. Salavati-Niasari, G. Hosseinzadeh, and F. Davar, *J. Alloys Compd.* **509**, 134 (2011).
23. J. Deng, L. Zhang, C. T. Au, and H. Dai, *Mater. Lett.* **63**, 632 (2009).
24. J. Liu, G. Wang, L. Lu, Y. Guo, and L. Yang, *RSC Adv.* **7**, 40965 (2017).
25. W. Nowicki, Z. S. Piskula, P. Kuźma, and P. Kirszensztejn, *J. Sol-Gel Sci. Technol.* **82**, 574 (2017).
26. C. Hu, H. Liu, W. Dong, Y. Zhang, G. Bao, C. Lao, and Z. L. Wang, *Adv. Mater.* **19**, 470 (2007).
27. F. Khosrow-Pour, M. Aghazadeh, S. Dalvand, and B. Sabour, *Mater. Lett.* **104**, 61 (2013).
28. Q. Liang, X. Yan, Y. Gu, K. Zhang, M. Liang, S. Lu, X. Zheng, and Y. Zhang, *Sci. Rep.* **5**, (2015).
29. Z. Wen, Q. Shen, and X. Sun, *Nano-Micro Lett.* **9**, (2017).
30. C. Zhang and Z. L. Wang, in (2018), pp. 1335–1376.
31. A. S. P. Dewi, N. Mufti, A. A. Fibriyanti, M. Diantoro, A. Taufiq, A. Hidayat, Sunaryono, and H. Nur, *J. Polym. Res.* **27**, (2020).

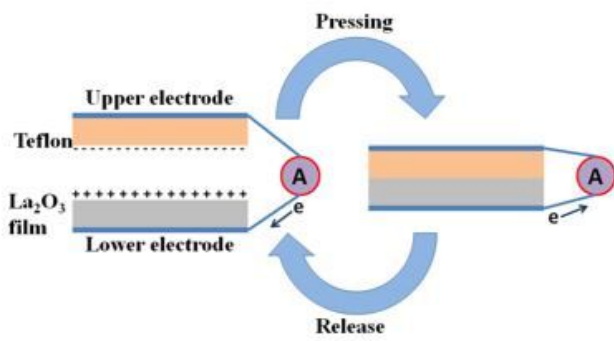
## Figures



(a)



(b)



(c)

Figure 1

(a) Image, (b) schematic representation of a motorized fixture for testing and (c) working principle of contact-separation mode of triboelectric response of La<sub>2</sub>O<sub>3</sub> film.

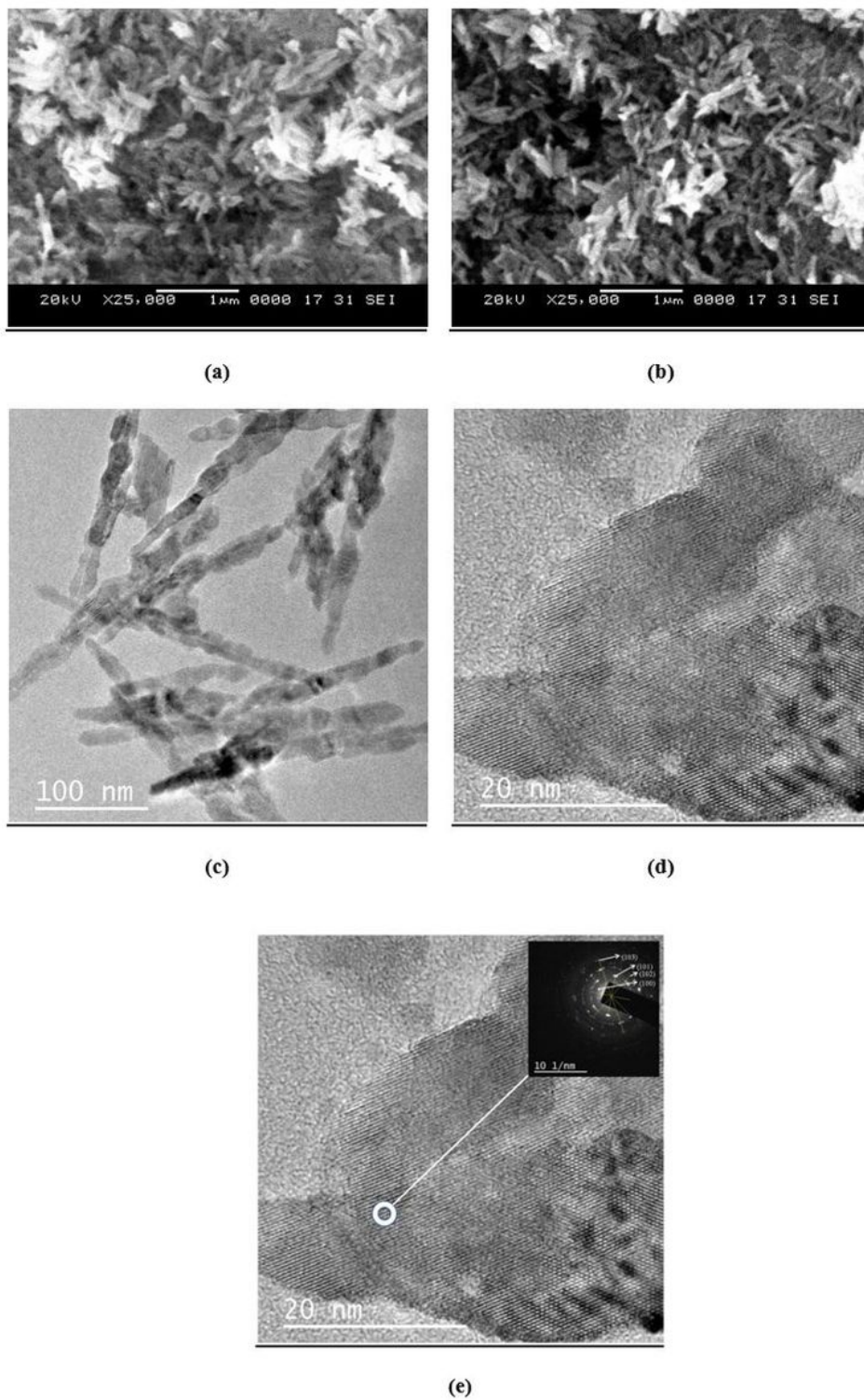


**Figure 2**

Morphology of La<sub>2</sub>O<sub>3</sub> nanocrystals captured using, (a) & (b) SEM, (c) TEM, (d) corresponding magnified high-resolution micrograph and (e) selected area electron diffraction (SAED) ring depicting the polycrystalline nature of La<sub>2</sub>O<sub>3</sub> nanocrystals.

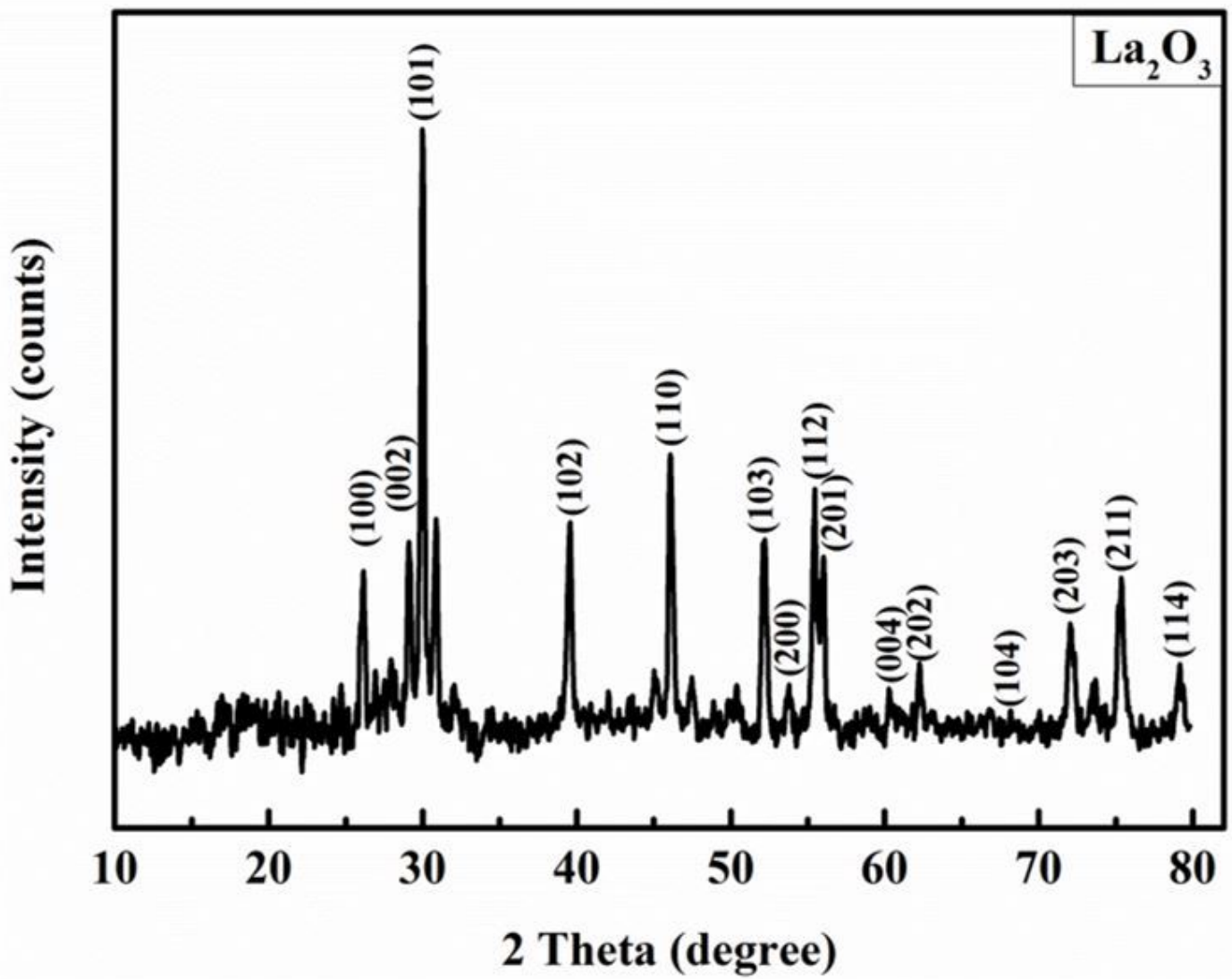
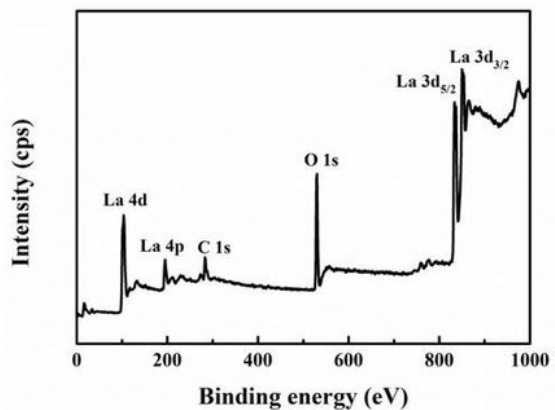
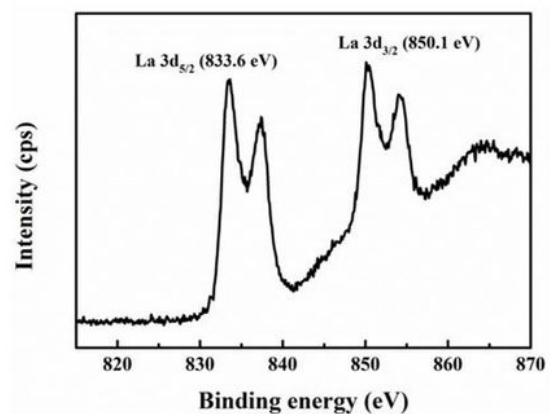


Figure 3

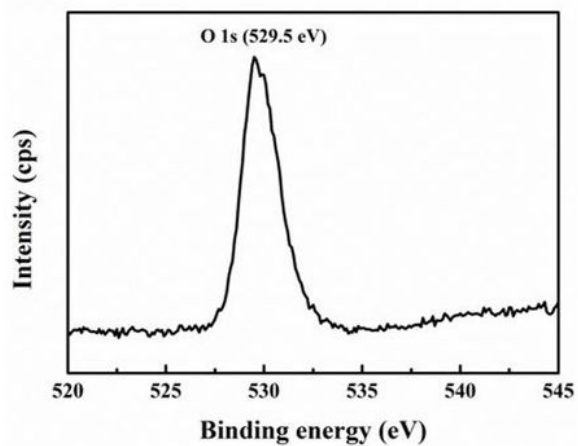
The XRD spectrum of hydrothermally synthesized La<sub>2</sub>O<sub>3</sub> nanocrystals.



(a)



(b)



(c)

**Figure 4**

XPS survey spectra of the La<sub>2</sub>O<sub>3</sub> showing both (a) low and high-resolution scans, (b) La 3d region and (c) O 1s region.

# MIT

Surface Area Analyser  
From Smart Instruments Co.Pvt.Ltd

Model: Smart Sorb 92/93  
WebSite: www.smartinstrument.com

Run Time:04:16 pm

Date:November 17 2017

% of N2 :30.7

Room temp.in Deg.C:25

Sample Name : La2O3

Wt of Tube (gms) :23.47

Wt of Tube+Sample (gms) :23.607

Sample Wt (gms) :.1370

Sample Wt after Reg. (gms) :.1260

Sample Loss : 8.0 %

Regeneration Temp.(deg.C) : 200

Time for regeneration (min.) :60

Desorption count : 31221.4

Injection count : 20958.2

Injected volume (cc) : 2.2

**Surface Area in (Sq.m/gm) : 72.33**

Remarks: | | |

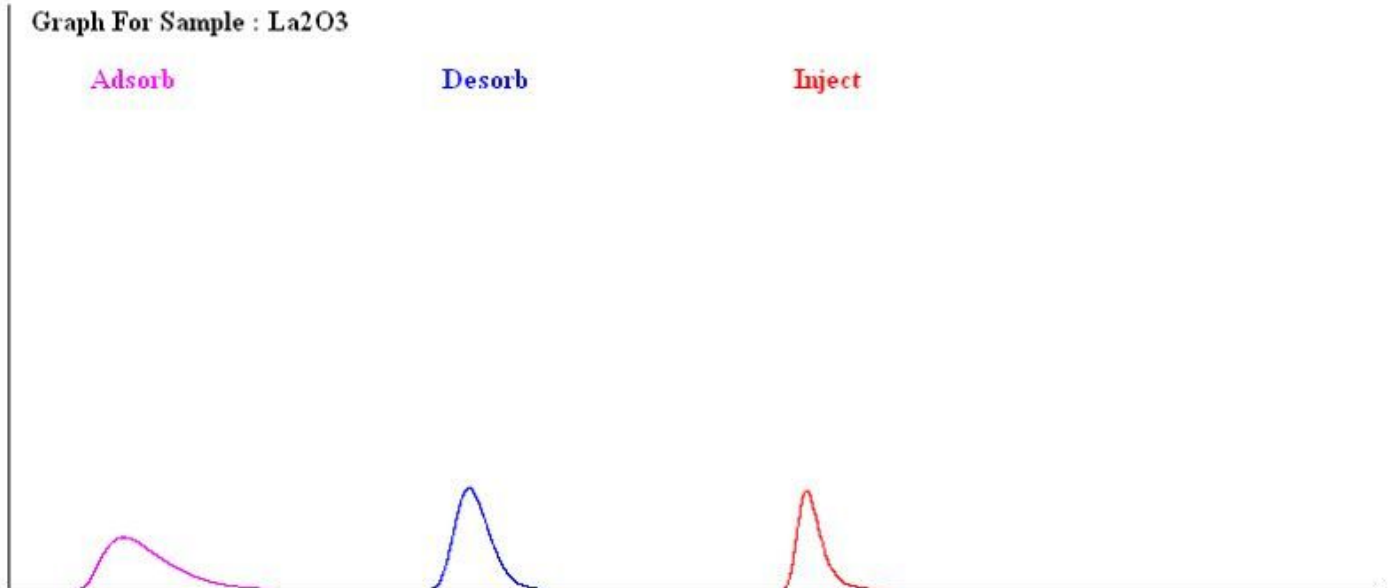


**Figure 5**

Nitrogen (N<sub>2</sub>) adsorption/desorption isotherms for La<sub>2</sub>O<sub>3</sub> nanocrystals.

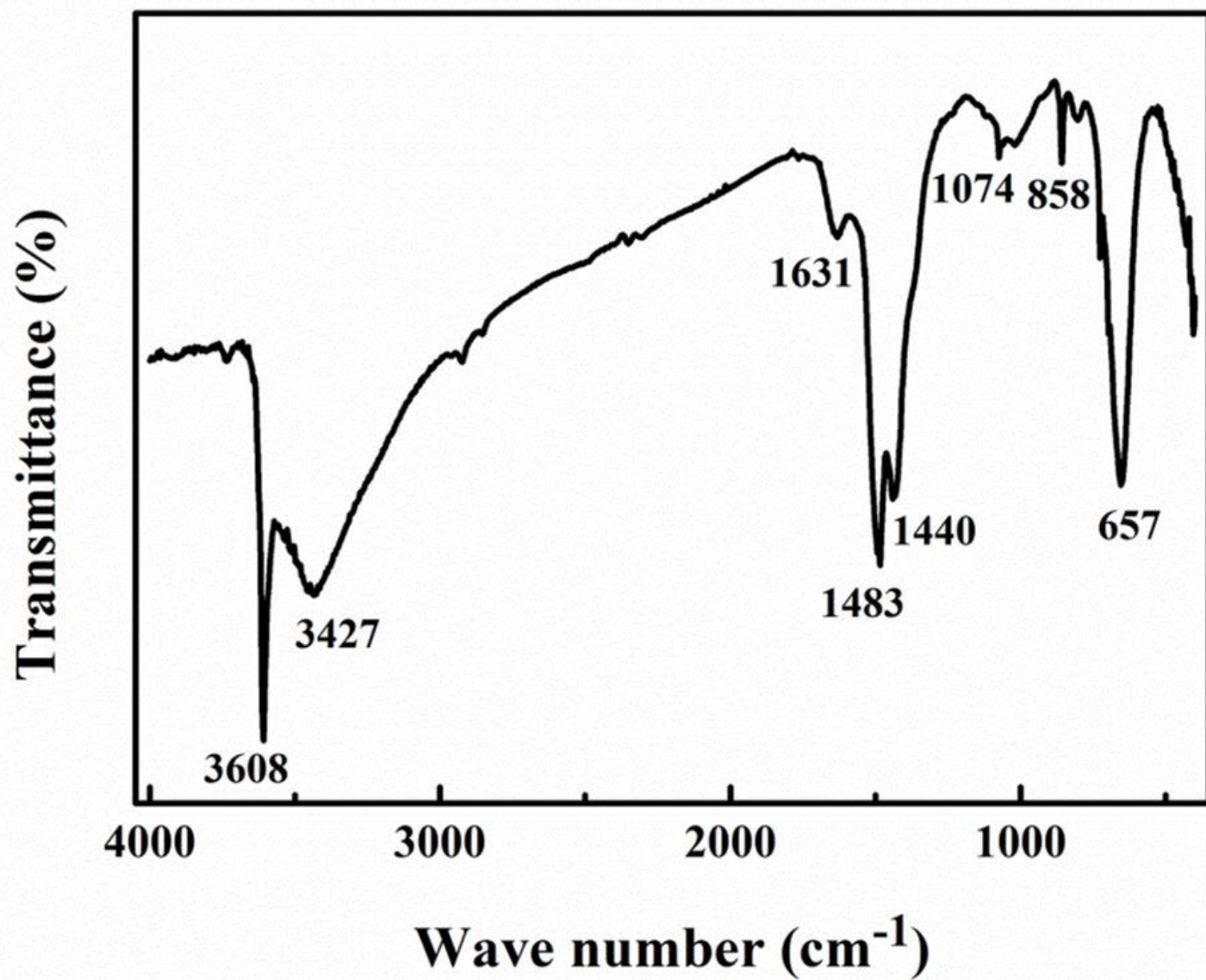


Figure 6

FTIR analysis of La<sub>2</sub>O<sub>3</sub> nanocrystals.

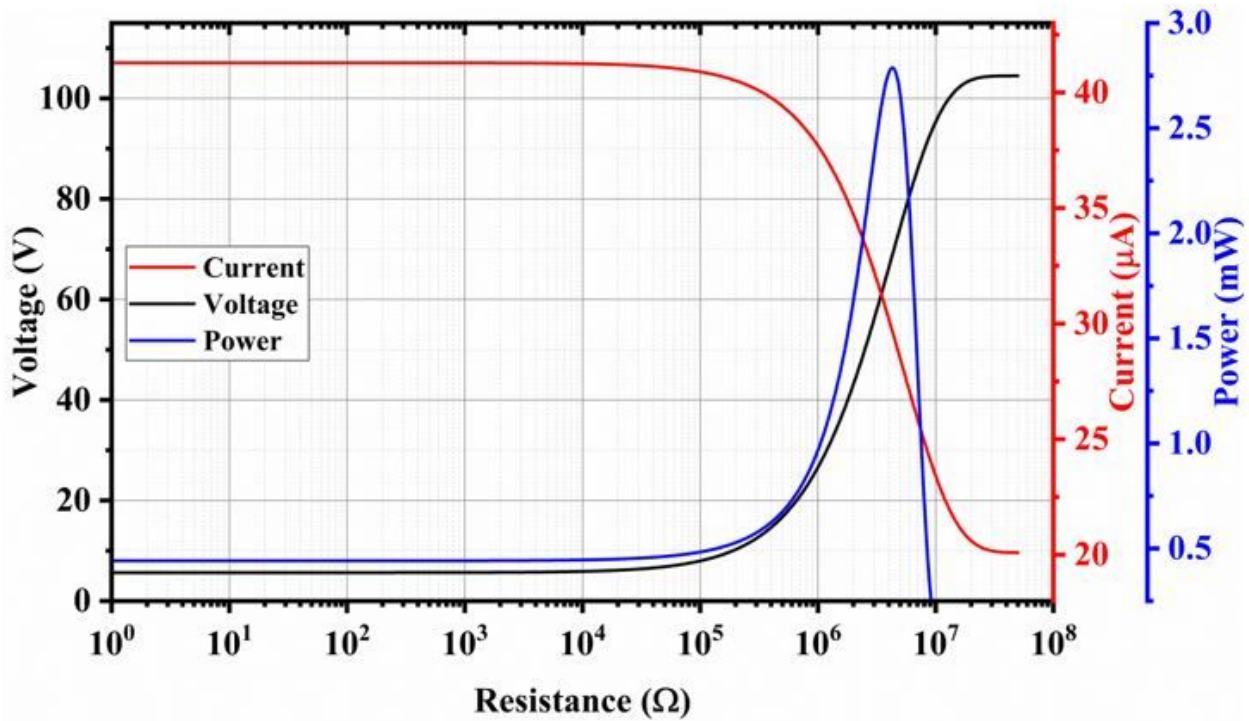
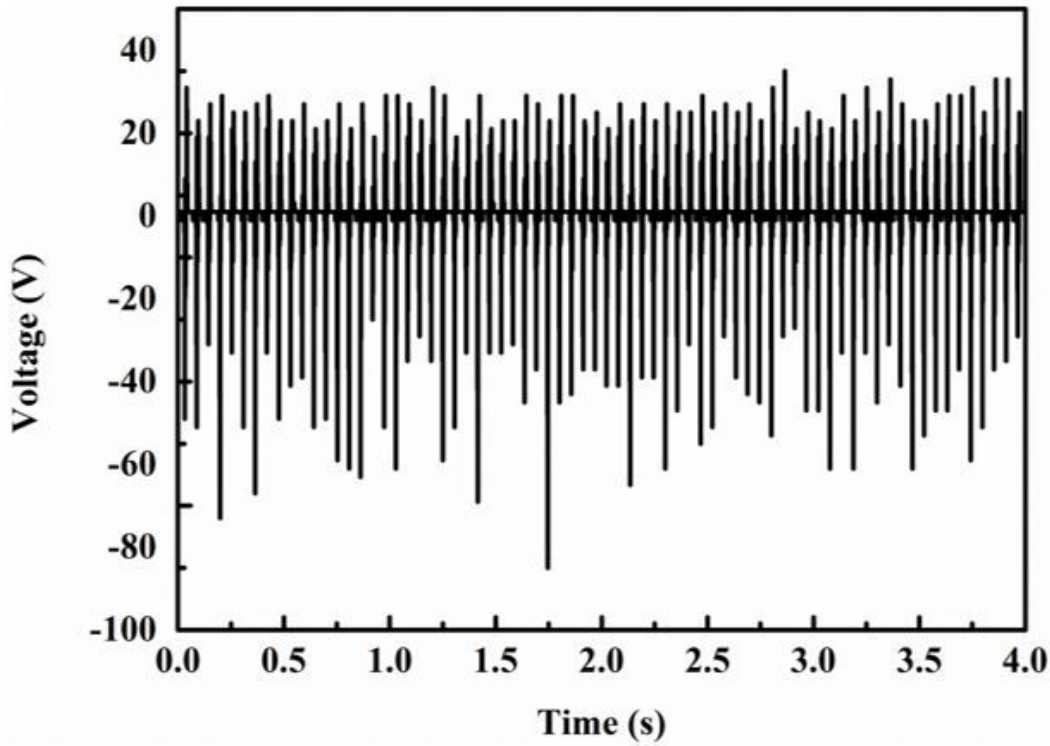


Figure 7

The characteristic electrical output of the La<sub>2</sub>O<sub>3</sub> triboelectric device showing its dependency of voltage and current output on external load resistance.

## Supplementary Files

This is a list of supplementary files associated with this preprint. Click to download.

- [Supplementaryinformation.docx](#)